# The Algebraic Cluster Model: Three-Body Clusters

R. Bijker

*Dipartimento di Fisica, Università degli Studi di Genova, Via Dodecaneso 33, I-16146 Genova, Italy;*[1] *Instituto de Ciencias Nucleares, Universidad Nacional Autónoma de México, Apartado Postal 70-543, 04510 México D.F., México*[2]
E-mail: bijker@nuclecu.unam.mx

and

F. Iachello

*Center for Thoretical Physics, Sloane Laboratory, Yale University, New Haven, Connecticut 06520-8120*
E-mail: francesco.iachello@yale.edu

Received January 21, 2002

A new method is introduced to study three-body clusters. Triangular configurations with $\mathcal{D}_{3h}$ point-group symmetry are analyzed. The spectrum, transition form factors, and $B(E\lambda)$ values of $^{12}$C are investigated. It is concluded that the low-lying spectrum of $^{12}$C can be described by three alpha-particles at the vertices of an equilateral triangle, but not as a rigid structure. Large rotation–vibration interactions, Coriolis forces, and vibration–vibration interactions are needed. Other interpretations, such as the harmonic oscillator and a soft deformed oscillator with $SO(6)$ hyperspherical symmetry, appear to be excluded by electron scattering data. 

*Key Words*: nuclear clusters; algebraic models.

## 1. INTRODUCTION

The cluster model of nuclei was introduced at the very beginning of nuclear physics as a natural consequence of the molecular viewpoint in which aggregates are formed by combining constituent units into composite objects. In particular, the alpha-particle model represented, for many years, a viable model of light nuclei [1]. With the successes of the nuclear shell model, the cluster model lost most of its appeal and the interest shifted to deriving the alpha-particle model from the nuclear shell model [2]. A large literature exists in this direction, especially from the Japanese school [3–5]. In recent years, clustering in nuclei has found renewed interest, since it appears that many new isotopes of light nuclei far from stability possess a cluster structure (not necessarily alpha). In view of this renewed interest, we have readdressed the question of clustering in nuclei with two purposes in mind. First, to analyze cluster configurations at the classical level in somewhat more detail than previously done, deriving explicit expressions for the density distribution and its multipole moments, and second, and most important, to introduce a formalism that allows one to study in a relatively simple fashion the actual situation which occurs in nuclei, where clustering is not a rigid-like molecular structure, but a rather soft (liquid-like) structure. The new approach is based

[1] Sabattical leave.
[2] Permanent address.



0003-4916/02 $35.00

the Lie algebra $U(\nu+1)$. This method has been used in a variety of problems, ranging from nuclear physics to molecular physics and from hadronic physics to polymer physics and has proven to be very useful in analyzing experimental data. In a series of articles beginning with the present one, we intend to exploit the algebraic method for cluster physics. Two-body clusters, where the algebra is $U(4)$, have been discussed previously [7]. Here we begin with three-body clusters, where the algebra is $U(7)$, and apply the method explicitly to the study of three-alpha configurations in nuclei, in particular to $^{12}$C. Many authors have suggested that this nucleus in its ground state is composed of three alpha-particles at the vertices of an equilateral triangle. In this article we study both at the classical and at the quantum level, a configuration of three particles at the vertices of an equilateral triangle (point-group symmetry $\mathcal{D}_{3h}$) and analyze the extent to which the experimental data support this configuration. A preliminary account of this part of our work has appeared [8, 9]. In addition to the study of properties of triangular configurations we also discuss other possible arrangements of three particles and their motion, in particular those corresponding to a six-dimensional spherical oscillator and to a six-dimensional deformed oscillator. Although these configurations do not appear to describe well the experimental data in $^{12}$C the formulas we derive may be of interest in other situations involving three particles.

## 2. CLASSICAL TREATMENT

The treatment of a triangular configuration in classical mechanics is very well known from molecular physics. However, this treatment is usually done in terms of point-like constituents. Although the generalization to composite constituents is straighforward, in this introductory section we present some new and more detailed results.

### 2.1. Energies

We consider three identical particles of mass $Am/3$ at the vertices of an equilateral triangle (point-group symmetry $\mathcal{D}_{3h}$) (see Fig. 1). The origin is placed at the center of mass and the three particles span the $xz$ plane. The distance from the center is $\beta$. The spherical coordinates of the three particles $\vec{r}_i = (r_i, \theta_i, \phi_i)$ are then $(\beta, 0, 0)$, $(\beta, 2\pi/3, \pi)$, and $(\beta, 2\pi/3, 0)$ for $i = 1, 2$, and 3, respectively. For a mass distribution $\rho(\vec{r})$, rotational energies can be computed by evaluating the moments of

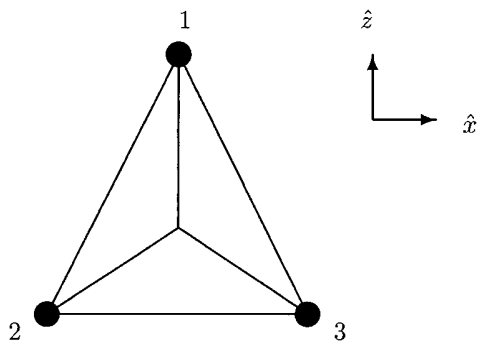


**FIG. 1.** Geometry of a three-body system.

$$\mathcal{I}_x = \int (y^2 + z^2)\rho(\vec{r})\, d\vec{r},$$
$$\mathcal{I}_y = \int (z^2 + x^2)\rho(\vec{r})\, d\vec{r}, \tag{2.1}$$
$$\mathcal{I}_z = \int (x^2 + y^2)\rho(\vec{r})\, d\vec{r}.$$

The rotational energy is simply

$$E_{\text{rot}} = \frac{1}{2\mathcal{I}_x}L_x^2 + \frac{1}{2\mathcal{I}_y}L_y^2 + \frac{1}{2\mathcal{I}_z}L_z^2. \tag{2.2}$$

2.1.1. *Point-like Masses*

For a point-like mass distribution

$$\rho(\vec{r}) = \frac{Am}{3}\sum_{i=1}^{3}\delta(\vec{r} - \vec{r}_i), \tag{2.3}$$

a simple calculation gives

$$\mathcal{I}_x = \mathcal{I}_z = \frac{1}{2}Am\beta^2,$$
$$\mathcal{I}_y = Am\beta^2, \tag{2.4}$$

and thus

$$E_{\text{rot}} = \frac{1}{Am\beta^2}\left[\vec{L}^2 - \frac{1}{2}K^2\right], \tag{2.5}$$

where $\vec{L}$ is the angular momentum and $K$ its projection on the three-fold $y$-axis.

2.1.2. *Extended Mass Distribution*

Consider the case in which instead of point masses there are, at the vertices of the triangle, extended distributions. Since we have in mind applications to the alpha-particle model, we consider here the case in which the distribution is Gaussian

$$\rho(\vec{r}) = \frac{Am}{3}\left(\frac{\alpha}{\pi}\right)^{3/2}\sum_{i=1}^{3}\exp[-\alpha(\vec{r} - \vec{r}_i)^2]. \tag{2.6}$$

It is straightforward to compute the moments of inertia

$$\mathcal{I}_x = \mathcal{I}_z = \frac{1}{2}Am\beta^2\left(1 + \frac{2}{\alpha\beta^2}\right),$$
$$\mathcal{I}_y = Am\beta^2\left(1 + \frac{1}{\alpha\beta^2}\right). \tag{2.7}$$

$$E_{\rm rot} = \frac{1}{Am\beta^2\left(1+\frac{2}{\alpha\beta^2}\right)}\left[\vec{L}^2 - \frac{\alpha\beta^2}{2(1+\alpha\beta^2)}K^2\right]. \tag{2.8}$$

For typical values of $\alpha$ and $\beta$, as for example those extracted from the form factors of $^{12}$C (discussed in the following sections), $\alpha = 0.52$ fm$^{-2}$, and $\beta = 1.74$ fm, we find that the coefficient in front of $K^2$ decreases from $-0.50$ to $-0.30$. We note in general that the rotational energy of a symmetric top is given by

$$E_{\rm rot} = A\vec{L}^2 + BK^2. \tag{2.9}$$

The top is called oblate if $B < 0$, prolate if $B > 0$, and spherical if $B = 0$. Three particles on a plane are always oblate. The extended distribution tends to make the top less oblate.

Vibrational energies can be computed by tying the particles with strings and evaluating the eigenfrequencies [10]. Denoting by $q_1$, $q_2$, and $q_3$ the displacements of the sides of the triangle and assuming a potential energy of the type

$$V = \frac{1}{2}C\left(q_1^2 + q_2^2 + q_3^2\right) + D(q_1q_2 + q_2q_3 + q_3q_1), \tag{2.10}$$

one can obtain the frequencies of the normal modes as

$$\begin{aligned} \omega_1 &= \sqrt{\frac{9(C+2D)}{Am}}, \\ \omega_2 &= \sqrt{\frac{9(C-D)}{2Am}}. \end{aligned} \tag{2.11}$$

The vibration $\omega_1$ is singly degenerate, while the vibration $\omega_2$ is doubly degenerate.

### 2.2. Transition Probabilities

Consider now the case in which the three particles have a charge $Ze/3$ (the case in which the particles have a magnetic moment will not be discussed here since we have in mind the alpha-particle model, where the constituents have no magnetic moment). The total charge distribution can be expanded into multipoles

$$\rho(\vec{r}) = \sum_{\ell m} A_{\ell m}(r)\, Y_{\ell m}(\theta, \phi), \tag{2.12}$$

with

$$A_{\ell m}(r) = \int Y^*_{\ell m}(\theta, \phi)\, \rho(\vec{r})\, d\cos\theta\, d\phi. \tag{2.13}$$

Instead of the charge distribution, one can consider the form factor, given by its Fourier transform

$$F(\vec{q}) = \frac{1}{Ze}\int e^{i\vec{q}\cdot\vec{r}}\, \rho(\vec{r})\, d\vec{r} = \sum_{\ell m} F_{\ell m}(q)\, Y_{\ell m}(\hat{q}), \tag{2.14}$$

$$F_{\ell m}(q) = \frac{4\pi}{Ze} \int r^2 \, A_{\ell m}(r) \, i^l \, j_\ell(qr) \, dr. \tag{2.15}$$

The multipole moments of the charge configuration are

$$\begin{aligned} Q_{\ell m} &= \int r^l \, Y^*_{\ell m}(\theta, \phi) \, \rho(\vec{r}) \, d\vec{r} = \int A_{\ell m}(r) \, r^{\ell+2} \, dr \\ &= \frac{Ze}{4\pi} (2\ell + 1)!! \lim_{q \to 0} \frac{F_{\ell m}(q)}{i^\ell q^\ell}. \end{aligned} \tag{2.16}$$

From these multipole moments, the transition probabilities can be calculated classically [11]. The transition probability per unit time is

$$T(E\ell) = 8\pi c \frac{e^2}{hc} \frac{\ell + 1}{\ell[(2\ell + 1)!!]^2} k^{2\ell+1} B(E\ell), \tag{2.17}$$

where

$$B(E\ell) = \sum_{m=-\ell}^{\ell} Q^*_{\ell m} Q_{\ell m}. \tag{2.18}$$

2.2.1. *Point Charges*

For a point-like charge distribution

$$\rho(\vec{r}) = \frac{Ze}{3} \sum_{i=1}^{3} \delta(\vec{r} - \vec{r}_i), \tag{2.19}$$

the form factor is given by

$$F(\vec{q}) = \frac{1}{3} \sum_{i=1}^{3} e^{i\vec{q} \cdot \vec{r}_i}. \tag{2.20}$$

The corresponding $B(E\ell)$ values are

$$B(E\ell) = \left(\frac{Ze}{3}\right)^2 \beta^{2\ell} \frac{2\ell + 1}{4\pi} \left[3 + 6P_\ell\left(-\frac{1}{2}\right)\right], \tag{2.21}$$

which gives

$$\begin{aligned} B(E2) &= (Ze)^2 \frac{5}{4\pi} \frac{1}{4} \beta^4, \\ B(E3) &= (Ze)^2 \frac{7}{4\pi} \frac{5}{8} \beta^6, \\ B(E4) &= (Ze)^2 \frac{9}{4\pi} \frac{9}{64} \beta^8. \end{aligned} \tag{2.22}$$

2.2.2. *Extended Charge Distributions*

Next we consider the case in which instead of point charges there are, at the vertices of the triangle, extended distributions

$$\rho(\vec{r}) = \frac{Ze}{3}\left(\frac{\alpha}{\pi}\right)^{3/2} \sum_{i=1}^{3} \exp[-\alpha(\vec{r}-\vec{r}_i)^2]$$
$$= \frac{Ze}{3}\left(\frac{\alpha}{\pi}\right)^{3/2} e^{-\alpha(r^2+\beta^2)}\, 4\pi \sum_{i=1}^{3}\sum_{\lambda=0}^{\infty} i_\lambda(2\alpha\beta r)\, Y_\lambda(\theta,\phi)\cdot Y_\lambda^*(\theta_i,\phi_i), \tag{2.23}$$

where $i_\lambda(x) = j_\lambda(ix)/i^\lambda$ is the modified spherical Bessel function. The corresponding form factor is that of the point-like charge distribution multiplied by an exponential

$$F(\vec{q}) = \frac{1}{3}\, e^{-q^2/4\alpha} \sum_{i=1}^{3} e^{i\vec{q}\cdot\vec{r}_i}. \tag{2.24}$$

The $B(E\ell)$ values of the extended charge distribution are the same as those of the point-like configuration.

## 3. QUANTUM TREATMENT

The quantum treatment of an identical three-body cluster can be done in several ways. The most straightforward is to introduce relative Jacobi coordinates

$$\vec{\rho} = (\vec{r}_1 - \vec{r}_2)/\sqrt{2},$$
$$\vec{\lambda} = (\vec{r}_1 + \vec{r}_2 - 2\vec{r}_3)/\sqrt{6}, \tag{3.1}$$

write down a Hamiltonian in terms of these coordinates and their canonically conjugate momenta $\vec{p}_\rho$ and $\vec{p}_\lambda$, and solve the Schrödinger equation

$$\left[\frac{1}{2m}\left(\vec{p}_\rho^{\,2} + \vec{p}_\lambda^{\,2}\right) + V(\vec{\rho},\vec{\lambda})\right]\psi(\vec{\rho},\vec{\lambda}) = E\,\psi(\vec{\rho},\vec{\lambda}) \tag{3.2}$$

to obtain the energy eigenvalues and eigenvectors.

### 3.1. Energies

It is convenient to make a change of variables to coordinates $(r, \xi, \Omega_\rho, \Omega_\lambda)$ which are related to the Jacobi coordinates $(\rho, \Omega_\rho, \lambda, \Omega_\lambda)$ by

$$\rho = r\sin\xi, \qquad \lambda = r\cos\xi. \tag{3.3}$$

$$-\frac{1}{2mr^5}\frac{\partial}{\partial r}\left(r^5\frac{\partial}{\partial r}\right)+\frac{1}{2mr^2}\left[-\frac{\partial^2}{\partial\xi^2}-4\cot 2\xi\,\frac{\partial}{\partial\xi}+\frac{\vec{L}_\rho^{\,2}(\Omega_\rho)}{\sin^2\xi}+\frac{\vec{L}_\lambda^{\,2}(\Omega_\lambda)}{\cos^2\xi}\right]. \tag{3.4}$$

In this section, we consider three different potentials, namely the harmonic oscillator, the deformed oscillator, and the oblate symmetric top. For potentials that only depend on the hyperradius $r$, the Schrödinger equation can be solved by separation of variables into an angular and a radial equation

$$\begin{gathered}\left[-\frac{\partial^2}{\partial\xi^2}-4\cot 2\xi\,\frac{\partial}{\partial\xi}+\frac{\vec{L}_\rho^{\,2}(\Omega_\rho)}{\sin^2\xi}+\frac{\vec{L}_\lambda^{\,2}(\Omega_\lambda)}{\cos^2\xi}\right]\psi(\xi,\Omega_\rho,\Omega_\lambda)=\sigma(\sigma+4)\,\psi(\xi,\Omega_\rho,\Omega_\lambda),\\ \left[-\frac{1}{2m}\frac{1}{r^5}\frac{\partial}{\partial r}\left(r^5\frac{\partial}{\partial r}\right)+\frac{\sigma(\sigma+4)}{2mr^2}+V(r)\right]\psi(r)=E\,\psi(r).\end{gathered} \tag{3.5}$$

For the six-dimensional harmonic oscillator

$$V(r)=\frac{1}{2}Cr^2, \tag{3.6}$$

the energy spectrum can be obtained exactly

$$E(n)=\epsilon(n+3), \tag{3.7}$$

with $n=0,1,\ldots,$ and $\epsilon=\sqrt{C/m}$. The allowed values of $\sigma$ are $\sigma=n,n-2,\ldots,1$ or 0 for $n$ odd or even, respectively.

For the six-dimensional displaced (or deformed) oscillator

$$V(r)=\frac{1}{2}C(r-r_0)^2, \tag{3.8}$$

the energy eigenvalues cannot be obtained exactly. An approximate solution, valid in the limit of small oscillations around the equilibrium value $r_0$, is

$$E(v,\sigma)\cong\epsilon\left(v+\frac{1}{2}\right)+\frac{1}{2mr_0^2}\left[\sigma(\sigma+4)+\frac{15}{4}\right], \tag{3.9}$$

with $\epsilon=\sqrt{C/m}$. The first term gives a harmonic vibrational spectrum with $v=0,1,\ldots,$ and the second term gives the rotational spectrum with $\sigma=0,1,\ldots$.

In general, the potential is not invariant under six-dimensional rotations as in the previous two examples, but only under rotations in three dimensions. One can introduce the total angular momentum $\vec{I}=\vec{L}_\rho+\vec{L}_\lambda$ and make a transformation of variables to the relative angle $2\theta$ between the two vectors

$$\cos 2\theta=\hat{\rho}\cdot\hat{\lambda} \tag{3.10}$$

and the Euler angles $\Omega$ of the intrinsic frame defined by [14]

$$\hat{1}=\frac{\hat{\rho}\times\hat{\lambda}}{\sin 2\theta},\qquad \hat{2}=\frac{\hat{\rho}-\hat{\lambda}}{2\sin\theta},\qquad \hat{3}=\frac{\hat{\rho}+\hat{\lambda}}{2\cos\theta}. \tag{3.11}$$

$$\frac{\vec{L}_\rho^2(\Omega_\rho)}{\sin^2\xi}+\frac{\vec{L}_\lambda^2(\Omega_\lambda)}{\cos^2\xi}=\frac{1}{4\sin^2\xi\cos^2\xi}\left(\vec{I}^{\,2}+\tan^2\theta\, I_2^2+\cot^2\theta\, I_3^2-\frac{\partial^2}{\partial\theta^2}-2\cot 2\theta\frac{\partial}{\partial\theta}\right)$$
$$+\frac{\cos 2\xi}{2\sin^2\xi\cos^2\xi}\left(-\cot\theta\, I_2 I_3-\tan\theta\, I_3 I_2+i I_1\frac{\partial}{\partial\theta}\right). \tag{3.12}$$

The potential only depends on the intrinsic variables $r$, $\xi$, and $\theta$. An interesting situation occurs when the potential has sharp minima in $r$, $\xi$, and $\theta$

$$V(r,\xi,\theta)=\frac{1}{2}C(r-r_0)^2+\frac{1}{2}A(\xi-\xi_0)^2+\frac{1}{2}B(\theta-\theta_0)^2. \tag{3.13}$$

In the limit of small oscillations around $r_0$, $\xi_0=\pi/4$, and $\theta_0=\pi/4$, rotations and vibrations decouple, and the set of resulting differential equations can be solved in closed form

$$E(v_1,v_{2a},v_{2b},I,K)\cong\epsilon_1\left(v_1+\frac{1}{2}\right)+\epsilon_{2a}\left(v_{2a}+\frac{1}{2}\right)+\epsilon_{2b}\left(v_{2b}+\frac{1}{2}\right)$$
$$+\frac{1}{mr_0^2}\left[I(I+1)-\frac{1}{2}K^2-\frac{9}{8}\right], \tag{3.14}$$

with $\epsilon_1=\sqrt{C/m}$, $\epsilon_{2a}=\sqrt{A/mr_0^2}$, and $\epsilon_{2b}=\sqrt{B/mr_0^2}$. Here $K$ is the projection of the angular momentum $I$ on the symmetry axis $\hat{1}$.

For three identical masses, the potential has to be invariant under their permutation; i.e., the coefficients $A$ and $B$ are equal. As a consequence, the vibrations $v_{2a}$ and $v_{2b}$ form a doubly degenerate vibration, and it is convenient to use instead of $v_{2a}$ and $v_{2b}$ the quantum numbers $v_2^{\ell_2}$ where $\ell_2=v_2,v_2-2,\ldots,1$ or 0 for $v_2=v_{2a}+v_{2b}$ odd or even. The vibrational energies can then be written as

$$E_{\rm vib}(v_1,v_2)=\epsilon_1\left(v_1+\frac{1}{2}\right)+\epsilon_2(v_2+1). \tag{3.15}$$

The rotational energies

$$E_{\rm rot}(I,K)=\frac{1}{mr_0^2}\left[I(I+1)-\frac{1}{2}K^2\right] \tag{3.16}$$

are the same as those derived classically for a triangular distribution of three identical point-like masses of Eq. (2.5) with $\vec{L}^2$ replaced by $I(I+1)$. The spectrum is that of an oblate symmetric top.

The triangular configuration with three identical masses has discrete symmetry $\mathcal{D}_{3h}$. Among the quantum numbers, it is convenient to add the parity $P$ and the transformation properties of the states under $\mathcal{D}_{3h}$. Since $\mathcal{D}_{3h}\sim\mathcal{D}_3\times P$, the transformation properties under $\mathcal{D}_{3h}$ are labeled by parity and the representations of $\mathcal{D}_3\sim S_3$. $\mathcal{D}_3$ has two one-dimensional representations, usually denoted by $A_1$ and $A_2$, and a two-dimensional representation denoted by $E$. The corresponding Young tableau of the permutation group $S_3$ are

$$t=A_1:\ \square\square\square \tag{3.17}$$

$$t = A_2 : \begin{array}{|c|}\hline \\ \hline \\ \hline \\ \hline \end{array} \tag{3.19}$$

For three identical particles, the wave functions must transform as the symmetric representations $A_1$ of $\mathcal{D}_3 \sim S_3$.

### 3.2. Transition Probabilities

Transition probabilities, charge radii, and other electromagnetic properties of interest can be obtained from the transition form factors. For electric transitions (the only ones discussed here) the form factors are the matrix elements of the Fourier transform of the charge distribution

$$F(i \to f; \vec{q}) = \int d\vec{r}\, e^{i\vec{q}\cdot\vec{r}} \langle \gamma_f, L_f, M_f | \hat{\rho}(\vec{r}) | \gamma_i, L_i, M_i \rangle, \tag{3.20}$$

where $\gamma$ denotes the extra quantum numbers needed to classify the states uniquely. For the point-like charge configuration of Eq. (2.19), the transition form factor reduces to

$$F(i \to f; \vec{q}) = Ze \sum_M \mathcal{D}^{(L_f)}_{M_f M}(\hat{q}) \mathcal{F}(i \to f; q) \mathcal{D}^{(L_i)}_{M M_i}(-\hat{q}), \tag{3.21}$$

with

$$\mathcal{F}(i \to f; q) = \langle \gamma_f, L_f, M | e^{-iq\sqrt{2/3}\lambda_z} | \gamma_i, L_i, M \rangle. \tag{3.22}$$

Here we have used the permutation symmetry of the initial and final wave functions, a transformation to Jacobi coordinates, and an integration over the center-of-mass coordinate. In Table I we show some form factors for the transition from the ground state to an excited state $\mathcal{F}(0_1^+ \to L_i^P; q)$. The form factors for the harmonic oscillator show an exponential dependence on the momentum transfer

TABLE I

Transition Form Factors $\mathcal{F}(0_1^+ \to L_i^P; q)$ for the Harmonic Oscillator (ho), the Deformed Oscillator (do), and the Oblate Top (ot)

| | $\mathcal{F}(0_1^+ \to L_i^P; q)$ | | |
|---|---|---|---|
| $L_i^P$ | ho | do | ot |
| $0_1^+$ | $e^{-q^2\beta^2/6}$ | $4\, J_2(q\beta\sqrt{2})/q^2\beta^2$ | $j_0(q\beta)$ |
| $0_2^+$ | $-\frac{1}{6\sqrt{3}}\, q^2\beta^2 e^{-q^2\beta^2/6}$ | 0 | $-\chi_1\, q\beta j_1(q\beta)$ |
| $1_1^-$ | $\frac{i}{6\sqrt{30}}\, q^3\beta^3 e^{-q^2\beta^2/6}$ | $i8\sqrt{3}\, J_5(q\beta\sqrt{2})/q^2\beta^2$ | $-i\chi_2\, \frac{1}{2}\sqrt{3}\, q\beta j_2(q\beta)$ |
| $2_1^+$ | $-\frac{1}{3\sqrt{6}}\, q^2\beta^2 e^{-q^2\beta^2/6}$ | $-8\sqrt{2}\, J_4(q\beta\sqrt{2})/q^2\beta^2$ | $\frac{1}{2}\sqrt{5}\, j_2(q\beta)$ |
| $3_1^-$ | $\frac{i}{18\sqrt{5}}\, q^3\beta^3 e^{-q^2\beta^2/6}$ | $i8\sqrt{2}\, J_5(q\beta\sqrt{2})/q^2\beta^2$ | $-i\sqrt{\frac{35}{8}}\, j_3(q\beta)$ |
| $4_1^+$ | $\frac{1}{18\sqrt{70}}\, q^4\beta^4 e^{-q^2\beta^2/6}$ | $\frac{48}{\sqrt{7}}\, J_6(q\beta\sqrt{2})/q^2\beta^2$ | $\frac{9}{8}\, j_4(q\beta)$ |

*Note*. For each case, a scale parameter $\beta$ was introduced to give the same result for the charge radius.

charge distribution of Eq. (2.23) can be obtained, as in the classical case, by multiplying the results from Table I by a Gaussian $\exp(-q^2/4\alpha)$, which represents the form factor of the $\alpha$ particle.

The transition probability $B(EL)$ can be extracted from the form factors in the long wavelength limit

$$B(EL; i \to f) = \frac{[(2L+1)!!]^2}{4\pi(2L_i+1)} \lim_{q\to 0} \sum_{M_f M_i} \frac{|F(i \to f; \vec{q})|^2}{q^{2L}}$$
$$= (Ze)^2 \frac{[(2L+1)!!]^2}{4\pi(2L_i+1)} \lim_{q\to 0} \sum_{M} \frac{|\mathcal{F}(i \to f; q)|^2}{q^{2L}}. \tag{3.23}$$

In the case of the oblate symmetric top, we find for the rotational excitations of the ground state the same results as for the multipole radiation in the classical case (see Eq. (2.22))

$$B(E2; 0^+ \to 2^+) = (Ze)^2 \frac{5}{4\pi} \frac{1}{4} \beta^4,$$
$$B(E3; 0^+ \to 3^-) = (Ze)^2 \frac{7}{4\pi} \frac{5}{8} \beta^6, \tag{3.24}$$
$$B(E4; 0^+ \to 4^+) = (Ze)^2 \frac{9}{4\pi} \frac{9}{64} \beta^8.$$

The ground state rotational band of the oblate top does not have a symmetric state with $L^P = 1^-$, which is in agreement with the absence of dipole radiation in the classical treatment.

The ground state charge distribution can be extracted from the elastic form factor by taking the Fourier transform

$$\rho(r) = \frac{1}{(2\pi)^3} \int d\vec{q}\, F(0_1^+ \to 0_1^+; \vec{q})\, e^{-i\vec{q}\cdot\vec{r}}$$
$$= \frac{Ze}{2\pi^2} \int q^2 dq\; j_0(qr)\, \mathcal{F}(0_1^+ \to 0_1^+; q). \tag{3.25}$$

For the case of the oblate top, the ground state charge distribution can be derived as

$$\rho(r) = Ze \left(\frac{\alpha}{\pi}\right)^{3/2} \frac{1}{4\alpha\beta r} \left[e^{-\alpha(\beta-r)^2} - e^{-\alpha(\beta+r)^2}\right]. \tag{3.26}$$

The charge radius can be obtained from the slope of the elastic form factor in the origin

$$\langle r^2 \rangle^{1/2} = \left[-6 \frac{d\mathcal{F}(0_1^+ \to 0_1^+; q)}{dq^2}\bigg|_{q=0}\right]^{1/2}. \tag{3.27}$$

In Table I we have introduced a scale parameter $\beta$ in the form factors, such that the charge radius for the harmonic oscillator, the deformed oscillator, and the oblate top is given by

$$\langle r^2 \rangle^{1/2} = \sqrt{\frac{3}{2\alpha} + \beta^2}. \tag{3.28}$$

In this section, we discuss an algebraic treatment of three-cluster systems, in which the eigenvalue problem is solved by matrix diagonalization instead of by solving a set of differential equations. In the algebraic cluster model (ACM), the method of bosonic quantization is used. This method consists in quantizing the Jacobi coordinates and momenta with boson operators and adding an additional scalar boson [15]

$$b^\dagger_{\rho,m}, \quad b^\dagger_{\lambda,m}, \quad s^\dagger \equiv c^\dagger_\alpha \qquad (m = 0, \pm 1) \quad (\alpha = 1, \ldots, 7). \tag{4.1}$$

The role of the additional scalar boson is to compactify the space, thus making calculations of matrix elements simpler. The set of 49 bilinear products of creation and annihilation operators spans the Lie algebra of $U(7)$

$$\mathcal{G} : G_{\alpha\beta} = c^\dagger_\alpha c_\beta \qquad (\alpha, \beta = 1, \ldots, 7). \tag{4.2}$$

All operators are expanded into elements of this algebra.

The most generic Hamiltonian which includes up to two-body terms and is invariant under the permutation group $S_3$, contains 10 parameters that describe the relative motion of a system of three identical clusters. It can be written as [15]

$$\begin{aligned} H = {} & \epsilon_0\, s^\dagger \tilde{s} - \epsilon_1 (b^\dagger_\rho \cdot \tilde{b}_\rho + b^\dagger_\lambda \cdot \tilde{b}_\lambda) + u_0\, (s^\dagger s^\dagger \tilde{s}\tilde{s}) - u_1\, s^\dagger (b^\dagger_\rho \cdot \tilde{b}_\rho + b^\dagger_\lambda \cdot \tilde{b}_\lambda)\tilde{s} \\ & + v_0 [(b^\dagger_\rho \cdot b^\dagger_\rho + b^\dagger_\lambda \cdot b^\dagger_\lambda)\tilde{s}\tilde{s} + s^\dagger s^\dagger (\tilde{b}_\rho \cdot \tilde{b}_\rho + \tilde{b}_\lambda \cdot \tilde{b}_\lambda)] \\ & + \sum_{l=0,2} w_l\, (b^\dagger_\rho \times b^\dagger_\rho + b^\dagger_\lambda \times b^\dagger_\lambda)^{(l)} \cdot (\tilde{b}_\rho \times \tilde{b}_\rho + \tilde{b}_\lambda \times \tilde{b}_\lambda)^{(l)} \\ & + \sum_{l=0,2} c_l \big[ (b^\dagger_\rho \times b^\dagger_\rho - b^\dagger_\lambda \times b^\dagger_\lambda)^{(l)} \cdot (\tilde{b}_\rho \times \tilde{b}_\rho - \tilde{b}_\lambda \times \tilde{b}_\lambda)^{(l)} \\ & + 4 (b^\dagger_\rho \times b^\dagger_\lambda)^{(l)} \cdot (\tilde{b}_\lambda \times \tilde{b}_\rho)^{(l)} \big] + c_1 (b^\dagger_\rho \times b^\dagger_\lambda)^{(1)} \cdot (\tilde{b}_\lambda \times \tilde{b}_\rho)^{(1)}, \end{aligned} \tag{4.3}$$

with $\tilde{b}_{\rho,m} = (-1)^{1-m} b_{\rho,-m}$, $\tilde{b}_{\lambda,m} = (-1)^{1-m} b_{\lambda,-m}$, and $\tilde{s} = s$. Here the dots indicate scalar products and the crosses tensor products with respect to the rotation group. By construction, the Hamiltonian commutes with the number operator

$$\hat{N} = s^\dagger \tilde{s} - b^\dagger_\rho \cdot \tilde{b}_\rho - b^\dagger_\lambda \cdot \tilde{b}_\lambda = s^\dagger s + \sum_m (b^\dagger_{\rho,m} b_{\rho,m} + b^\dagger_{\lambda,m} b_{\lambda,m}) \tag{4.4}$$

and therefore conserves the total number of bosons $N = n_s + n_\rho + n_\lambda$. In addition to $N$, the eigenfunctions have good angular momentum $L$, parity $P$, and permutation symmetry $t$. The three symmetry classes of the $S_3$ permutation group are characterized by the irreducible representations: $t = S$ for the one-dimensional symmetric representation, $t = A$ for the one-dimensional antisymmetric representation, and $t = M$ for the two-dimensional mixed symmetry representation.

### 4.1. Dynamic Symmetries

The $S_3$ invariant $U(7)$ mass operator of Eq. (4.3) has a rich algebraic structure. It is of general interest to study limiting situations, in which the energy spectra can be obtained in closed form. These special cases correspond to dynamic symmetries of the Hamiltonian. Dynamic symmetries arise, when (i) the Hamiltonian has an algebraic structure $G$, and (ii) it can be expressed in terms of Casimir invariants of a chain of subalgebras of $G$ only. Here we consider two different dynamic

For $v_0 = 0$ in Eq. (4.3), we recover the six-dimensional oscillator model, since there is no coupling between different harmonic oscillator shells. The oscillator is harmonic if all terms except $\epsilon_0$ and $\epsilon_1$ are set to zero; otherwise it is anharmonic. This dynamic symmetry corresponds to the reduction

$$U(7) \supset U(6) \supset SO(6) \supset \cdots. \tag{4.5}$$

The dots here indicate further subalgebras needed to classify the states uniquely. Since our purpose here is to present a global analysis of the situation, we do not dwell on the group theoretical aspects of this problem and rather note that the one-body Hamiltonian

$$\begin{aligned} H_1 &= -\epsilon_1 (b^\dagger_\rho \cdot \tilde{b}_\rho + b^\dagger_\lambda \cdot \tilde{b}_\lambda) \\ &= \epsilon_1 \sum_m (b^\dagger_{\rho,m} b_{\rho,m} + b^\dagger_{\lambda,m} b_{\lambda,m}) \\ &= \epsilon_1 \hat{C}_{1U(6)} \end{aligned} \tag{4.6}$$

gives the energy spectrum of a six-dimensional spherical oscillator

$$E_1(n) = \epsilon_1 n. \tag{4.7}$$

Here $\hat{C}_{1U(6)}$ denotes the linear Casimir operator of $U(6)$. The label $n$ represents the number of oscillator quanta $n = n_\rho + n_\lambda = 0, 1, \ldots, N$. This special case is called the $U(6)$ limit. In Fig. 2 we show the structure of the spectrum of the spherical harmonic oscillator with $U(6)$ symmetry. For three identical clusters, the wave functions must transform as the symmetric representation $t = S$ of the permutation group $S_3$. The levels are grouped into oscillator shells characterized by $n$. In Fig. 2, the levels belonging to an oscillator shell $n$ are further classified by $\sigma = n, n-2, \ldots, 1$ or 0 for $n$ odd or even. The quantum number $\sigma$ labels the representations of $SO(6)$, a subgroup of $U(6)$. The ground state has $n = 0$ and $L^P = 0^+$. We note that the $n = \sigma = 1$ shell is absent, since it does not contain a symmetric state with $t = S$. The two-phonon multiplet $n = 2$ consists of the states $L^P = 2^+$ with $\sigma = 2$ and $0^+$ with $\sigma = 0$. The degeneracy of the harmonic oscillator shells can be split by adding invariants of subgroups of $U(6)$ [17].

For the six-dimensional spherical oscillator, the number of oscillator quanta $n$ is a good quantum number. However, when $v_0 \neq 0$ in Eq. (4.3), the oscillator shells with $\Delta n = \pm 2$ are mixed, and the eigenfunctions are spread over many different oscillator shells. A dynamic symmetry that involves the mixing between oscillator shells is provided by the reduction

$$U(7) \supset SO(7) \supset SO(6) \supset \cdots. \tag{4.8}$$

Again the dots indicate further subalgebras needed to classify the states uniquely. They can be taken as discussed previously. We consider now an algebraic Hamiltonian of the form

$$\begin{aligned} H_2 &= \kappa[\hat{N}(\hat{N}+5) - (\hat{D}_\rho \cdot \hat{D}_\rho + \hat{D}_\lambda \cdot \hat{D}_\lambda)] \\ &= \kappa\left[\hat{N}(\hat{N}+5) - \hat{C}_{2SO(7)} + \hat{C}_{2SO(6)}\right] \\ &= \kappa\left[(s^\dagger s^\dagger - b^\dagger_\rho \cdot b^\dagger_\rho - b^\dagger_\lambda \cdot b^\dagger_\lambda)(\tilde{s}\tilde{s} - \tilde{b}_\rho \cdot \tilde{b}_\rho - \tilde{b}_\lambda \cdot \tilde{b}_\lambda) + \hat{C}_{2SO(6)}\right], \end{aligned} \tag{4.9}$$

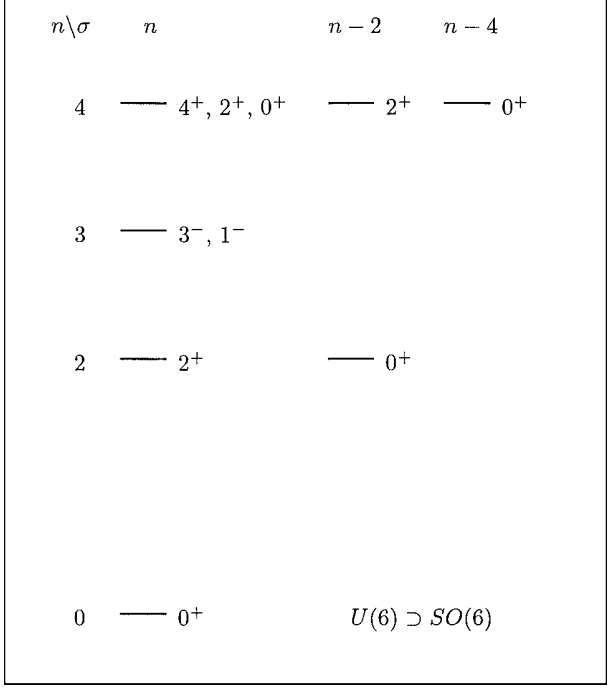


**FIG. 2.** Schematic spectrum of the harmonic oscillator with $U(6) \supset SO(6)$ symmetry. The number of bosons is $N = 4$. All states are symmetric under $S_3$.

where $\hat{N}$ is the number operator of Eq. (4.4) and $\hat{D}$ denote the dipole operators

$$\begin{aligned} \hat{D}_{\rho,m} &= (b^\dagger_\rho \times \tilde{s} - s^\dagger \times \tilde{b}_\rho)^{(1)}_m, \\ \hat{D}_{\lambda,m} &= (b^\dagger_\lambda \times \tilde{s} - s^\dagger \times \tilde{b}_\lambda)^{(1)}_m. \end{aligned} \tag{4.10}$$

The operators $\hat{C}_{2SO(7)}$ and $\hat{C}_{2SO(6)}$ represent the quadratic Casimir operators of $SO(7)$ and $SO(6)$, respectively. The energy spectrum in this case, called the $SO(7)$ limit, is given by the eigenvalues of the Casimir operators $\langle \hat{C}_{2SO(7)} \rangle = \omega(\omega + 5)$ and $\langle \hat{C}_{2SO(6)} \rangle = \sigma(\sigma + 4)$

$$E_2(\omega, \sigma) = \kappa \, [(N - \omega)(N + \omega + 5) + \sigma(\sigma + 4)]. \tag{4.11}$$

Here $\omega = N, N-2, \ldots, 1$ or 0 for $N$ odd or even, respectively, labels the symmetric representations of $SO(7)$, and $\sigma = 0, 2, 3, \ldots, \omega$ those of $SO(6)$ (note that $\sigma = 1$ is missing, since it does not contain a symmetric state). The correspondence with the energy spectrum of the deformed oscillator of Eq. (3.9) can be seen by introducing a vibrational quantum number $v = (N - \omega)/2$. The energy formula reduces to

$$E_2(v, \sigma) = 4\kappa N v \left(1 - \frac{2v - 5}{2N}\right) + \kappa\sigma(\sigma + 4), \tag{4.12}$$

which to leading order in $N$ is linear in the vibrational quantum number. In Fig. 3 we show the

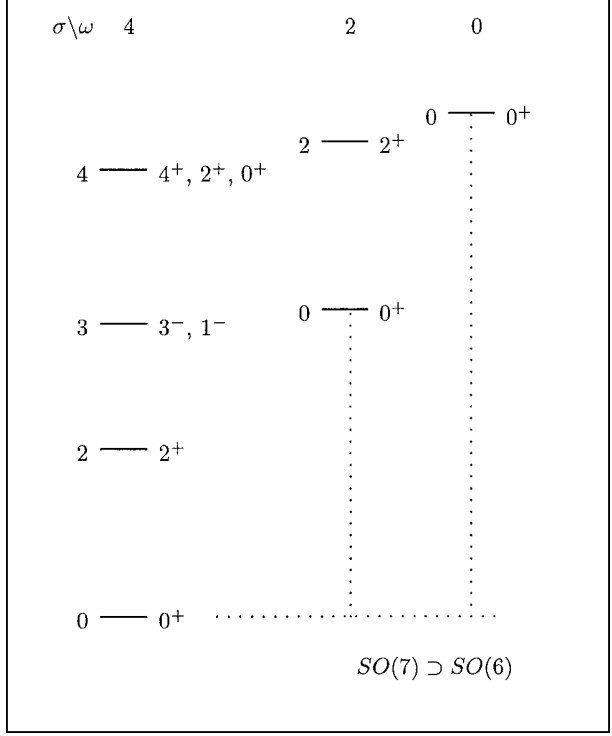


**FIG. 3.** Schematic spectrum of a deformed oscillator with $SO(7)$ symmetry. The number of bosons is $N = 4$. All states are symmetric under $S_3$.

spectrum of the deformed oscillator with $SO(7)$ symmetry. The states are now ordered in bands labeled by $\omega$, rather than in harmonic oscillator shells. Although the size of the model space, and hence the total number of states, is the same as for the harmonic oscillator, the ordering and classification of the states are different. For example, in the $U(6)$ limit all states are vibrational, whereas the $SO(7)$ limit gives rise to a rotational–vibrational spectrum, characterized by a series of rotational bands which are labeled by $\omega$, or equivalently by the vibrational quantum number $v = (N - \omega)/2 = 0, 1, \ldots$.

### 4.2. Oblate Symmetric Top

This situation does not correspond to a dynamic symmetry of the Hamiltonian $H$. However it is relatively simple to construct an algebraic Hamiltonian that produces the spectrum of an oblate symmetric top. This Hamiltonian was suggested in our preliminary account of this work [8]. It can be written as

$$\begin{aligned} H_3 = {} & \xi_1(s^\dagger s^\dagger - b_\rho^\dagger \cdot b_\rho^\dagger - b_\lambda^\dagger \cdot b_\lambda^\dagger)(\tilde{s}\tilde{s} - \tilde{b}_\rho \cdot \tilde{b}_\rho - \tilde{b}_\lambda \cdot \tilde{b}_\lambda) \\ & + \xi_2[(b_\rho^\dagger \cdot b_\rho^\dagger - b_\lambda^\dagger \cdot b_\lambda^\dagger)(\tilde{b}_\rho \cdot \tilde{b}_\rho - \tilde{b}_\lambda \cdot \tilde{b}_\lambda) + 4(b_\rho^\dagger \cdot b_\lambda^\dagger)(\tilde{b}_\lambda \cdot \tilde{b}_\rho)] \\ & + 2\kappa_1(b_\rho^\dagger \times \tilde{b}_\rho + b_\lambda^\dagger \times \tilde{b}_\lambda)^{(1)} \cdot (b_\rho^\dagger \times \tilde{b}_\rho + b_\lambda^\dagger \times \tilde{b}_\lambda)^{(1)} \\ & + 3\kappa_2(b_\rho^\dagger \times \tilde{b}_\lambda - b_\lambda^\dagger \times \tilde{b}_\rho)^{(0)} \cdot (b_\lambda^\dagger \times \tilde{b}_\rho - b_\rho^\dagger \times \tilde{b}_\lambda)^{(0)}. \end{aligned} \tag{4.13}$$

one of us (RB) and is available upon request [19]. An approximate energy formula can be obtained by making use of the method of intrinsic or coherent states as discussed in the following section.

## 5. GEOMETRIC ANALYSIS

The geometric properties of the general algebraic Hamiltonian $H$ of Eq. (4.3) can be studied by using intrinsic or coherent states [20]. The ground state coherent state for the problem at hand can be written as

$$|N;\vec{\alpha}_\rho,\vec{\alpha}_\lambda\rangle = \frac{1}{\sqrt{N!}}(b_c^\dagger)^N\,|0\rangle, \tag{5.1}$$

with

$$b_c^\dagger = \sqrt{1-\vec{\alpha}_\rho\cdot\vec{\alpha}_\rho^*-\vec{\alpha}_\lambda\cdot\vec{\alpha}_\lambda^*}\;s^\dagger+\vec{\alpha}_\rho\cdot\vec{b}_\rho^\dagger+\vec{\alpha}_\lambda\cdot\vec{b}_\lambda^\dagger. \tag{5.2}$$

The condensate boson Eq. (5.2) is parametrized in terms of two vectors, $\vec{\alpha}_\rho$ and $\vec{\alpha}_\lambda$, which can be transformed to intrinsic coordinates $q_\rho$, $\theta_\rho$, $\phi_\rho$ and $q_\lambda$, $\theta_\lambda$, $\phi_\lambda$, and their conjugate momenta [21]

$$\alpha_{k,\mu} = \frac{1}{\sqrt{2}}\sum_\nu \mathcal{D}^{(1)}_{\mu\nu}(\phi_k,\theta_k,0)\,\beta_{k,\nu}, \tag{5.3}$$

with

$$\begin{pmatrix}\beta_{k,1}\\ \beta_{k,0}\\ \beta_{k,-1}\end{pmatrix} = \begin{pmatrix}\left[-p_{\phi_k}/\sin\theta_k - ip_{\theta_k}\right]/q_k\sqrt{2}\\ q_k+ip_k\\ \left[-p_{\phi_k}/\sin\theta_k + ip_{\theta_k}\right]/q_k\sqrt{2}\end{pmatrix}, \tag{5.4}$$

with $k=\rho,\lambda$. The classical limit of a normal ordered operator can be defined as the coherent state expectation value of the operator divided by the number of bosons $N$.

### 5.1. Dynamic Symmetries

We start by analyzing the two dynamic symmetries discussed in the previous section. For the $U(6)$ limit, the classical limit of the Hamiltonian is given by

$$\begin{aligned} H_{1,\mathrm{cl}} &= \frac{1}{N}\langle N;\vec{\alpha}_\rho,\vec{\alpha}_\lambda\,|:H_1:|\,N;\vec{\alpha}_\rho,\vec{\alpha}_\lambda\rangle \\ &= \epsilon_1\,(\vec{\alpha}_\rho\cdot\vec{\alpha}_\rho^*+\vec{\alpha}_\lambda\cdot\vec{\alpha}_\lambda^*) \\ &= \epsilon_1\frac{1}{2}\big(p_\rho^2+q_\rho^2+\vec{L}_\rho^2/q_\rho^2+p_\lambda^2+q_\lambda^2+\vec{L}_\lambda^2/q_\lambda^2\big), \end{aligned} \tag{5.5}$$

where $\vec{L}_k^2$ is the angular momentum in polar coordinates

$$\vec{L}_k^2 = p_{\theta_k}^2+\frac{p_{\phi_k}^2}{\sin^2\theta_k}, \tag{5.6}$$

For the $SO(7)$ limit, we find

$$H_{2,\mathrm{cl}} = \kappa(N-1)\left[q^2p^2 + (1-q^2)^2 - \frac{\partial^2}{\partial\chi^2} - 4\cot 2\chi\frac{\partial}{\partial\chi} + \frac{\vec{L}_\rho^2}{\sin^2\chi} + \frac{\vec{L}_\lambda^2}{\cos^2\chi}\right]. \tag{5.7}$$

Here we have made a change to hyperspherical variables

$$q_\rho = q\sin\chi, \qquad q_\lambda = q\cos\chi \tag{5.8}$$

and their conjugate momenta. In the limit of small oscillations around the minimum of the potential energy surface $q = 1 + \Delta q$ we find to leading order in $N$ a one-dimensional harmonic oscillator in the hyperradius $q$

$$H_{2,\mathrm{cl}} \to \kappa N(p^2 + 4(\Delta q)^2), \tag{5.9}$$

with frequency $4\kappa N$. To leading order in $N$, the frequency coincides with that of Eq. (4.12). This analysis shows the connection between the $SO(7)$ dynamical symmetry and the displaced oscillator.

### 5.2. Oblate Symmetric Top

For the oblate symmetric top, the method of intrinsic states becomes particularly useful, since this case does not correpond to a dynamic symmetry. We first consider the vibrational part of the Hamiltonian of Eq. (4.13)

$$\begin{aligned} H_{3,\mathrm{vib}} = {} & \xi_1(R^2 s^\dagger s^\dagger - b_\rho^\dagger\cdot b_\rho^\dagger - b_\lambda^\dagger\cdot b_\lambda^\dagger)(R^2\tilde{s}\tilde{s} - \tilde{b}_\rho\cdot\tilde{b}_\rho - \tilde{b}_\lambda\cdot\tilde{b}_\lambda) \\ & + \xi_2[(b_\rho^\dagger\cdot b_\rho^\dagger - b_\lambda^\dagger\cdot b_\lambda^\dagger)(\tilde{b}_\rho\cdot\tilde{b}_\rho - \tilde{b}_\lambda\cdot\tilde{b}_\lambda) + 4(b_\rho^\dagger\cdot b_\lambda^\dagger)(\tilde{b}_\lambda\cdot\tilde{b}_\rho)]. \end{aligned} \tag{5.10}$$

For $R^2 = 0$, this Hamiltonian has $U(7) \supset U(6)$ symmetry and corresponds to a spherical vibrator, whereas for $R^2 = 1$ and $\xi_2 = 0$ it has $U(7) \supset SO(7)$ symmetry and corresponds to a deformed oscillator. Here we analyze the general case with $R^2 \neq 0$ and $\xi_1, \xi_2 > 0$. The classical limit of the Hamiltonian of Eq. (5.10) has a complicated structure. The equilibrium configuration of the potential energy surface is given by

$$q_0 = \sqrt{2R^2/(1+R^2)}, \qquad \chi_0 = \pi/4, \qquad \zeta_0 = \pi/4, \tag{5.11}$$

where the relative angle between $\vec{\alpha}_\rho$ and $\vec{\alpha}_\lambda$ is denoted by $2\zeta$. In the limit of small oscillations around the minimum $q = q_0 + \Delta q$, $\chi = \chi_0 + \Delta\chi$ and $\zeta = \zeta_0 + \Delta\zeta$, the intrinsic degrees of freedom $q$, $\chi$, and $\zeta$ decouple and become harmonic. To leading order in $N$ we find

$$\begin{aligned} H_{3,\mathrm{cl}} = {} & \xi_1 N\left[\frac{2R^2}{1+R^2}p^2 + 2R^2(1+R^2)(\Delta q)^2\right] \\ & + \xi_2 N\left[p_\chi^2 + \frac{4R^4}{(1+R^2)^2}(\Delta\chi)^2 + p_\zeta^2 + \frac{4R^4}{(1+R^2)^2}(\Delta\zeta)^2\right]. \end{aligned} \tag{5.12}$$

$$E_{3,\mathrm{vib}}(v_1, v_2) = \omega_1\left(v_1 + \frac{1}{2}\right) + \omega_2(v_2 + 1), \tag{5.13}$$

with frequencies

$$\omega_1 = 4NR^2\xi_1, \qquad \omega_2 = \frac{4NR^2}{1+R^2}\xi_2, \tag{5.14}$$

in agreement with the results obtained in a normal mode analysis [15]. Here $v_1$ and $v_2$ represent vibrational quantum numbers for a one- and two-dimensional harmonic oscillator, respectively.

We consider next the rotational part of the Hamiltonian which can be rewritten as

$$\begin{aligned} H_{3,\mathrm{rot}} = {} & 2\kappa_1(b_\rho^\dagger \times \tilde{b}_\rho + b_\lambda^\dagger \times \tilde{b}_\lambda)^{(1)} \cdot (b_\rho^\dagger \times \tilde{b}_\rho + b_\lambda^\dagger \times \tilde{b}_\lambda)^{(1)} \\ & + 3\kappa_2(b_\rho^\dagger \times \tilde{b}_\lambda - b_\lambda^\dagger \times \tilde{b}_\rho)^{(0)} \cdot (b_\lambda^\dagger \times \tilde{b}_\rho - b_\rho^\dagger \times \tilde{b}_\lambda)^{(0)}. \end{aligned} \tag{5.15}$$

Both terms commute with the general $S_3$ invariant Hamiltonian of Eq. (4.3) and hence correspond to exact symmetries. The eigenvalues are given by

$$\begin{aligned} E_{3,\mathrm{rot}} &= \kappa_1 L(L+1) + \kappa_2 m_F^2 \\ &= \kappa_1 L(L+1) + \kappa_2 (K \mp 2\ell_2)^2. \end{aligned} \tag{5.16}$$

Here we have used that for the oblate top the quantum number $m_F$ is related to the projection $K$ of the angular momentum on the symmetry axis and $\ell_2$ [22]. The last term contains the effects of the Coriolis force which gives rise to a $8\kappa_2 K\ell_2$ splitting of the rotational levels.

The total (rotation–vibration) wave functions of a rigid triangular configuration can be written as

$$\left|\left(v_1, v_2^{\ell_2}\right); K, L_t^P, M\right\rangle. \tag{5.17}$$

For three identical particles, the wave functions for rigid configurations must transform as the symmetric representations $A_1$ of $\mathcal{D}_3 \sim S_3$. This imposes some conditions on the allowed values of the angular momenta. For vibrational bands with $\ell_2 = 0$ and 1, the allowed values of the angular momenta are

$$\begin{array}{lll} \left(v_1, v_2^{\ell_2=0}\right): & K = 3n & n = 0, 1, 2, \ldots \\ & L = 0, 2, 4, \ldots & \text{for } K = 0 \\ & L = K, K+1, K+2, \ldots & \text{for } K \neq 0 \\ \left(v_1, v_2^{\ell_2=1}\right): & K = 3n+1, 3n+2 & n = 0, 1, 2, \ldots \\ & L = K, K+1, K+2, \ldots. & \end{array} \tag{5.18}$$

The parity is $P = (-)^K$. The vibrational band $(1, 0^0)$ has the same angular momenta $L^P = 0^+$, $2^+, 3^-, 4^\pm, \ldots$, as the ground state band $(0, 0^0)$, while the angular momentum content of the doubly degenerate vibration $(0, 1^1)$ is given by $L^P = 1^-, 2^\mp, 3^\mp, \ldots$. Combining all results one can write an approximate expression for the energy eigenvalues for the oblate symmetric top

$$E\left(v_1, v_2^{\ell_2}, K, L, M\right) = E_0 + \omega_1\left(v_1 + \frac{1}{2}\right) + \omega_2(v_2+1) + \kappa_1 L(L+1) + \kappa_2(K \mp 2\ell_2)^2. \tag{5.19}$$

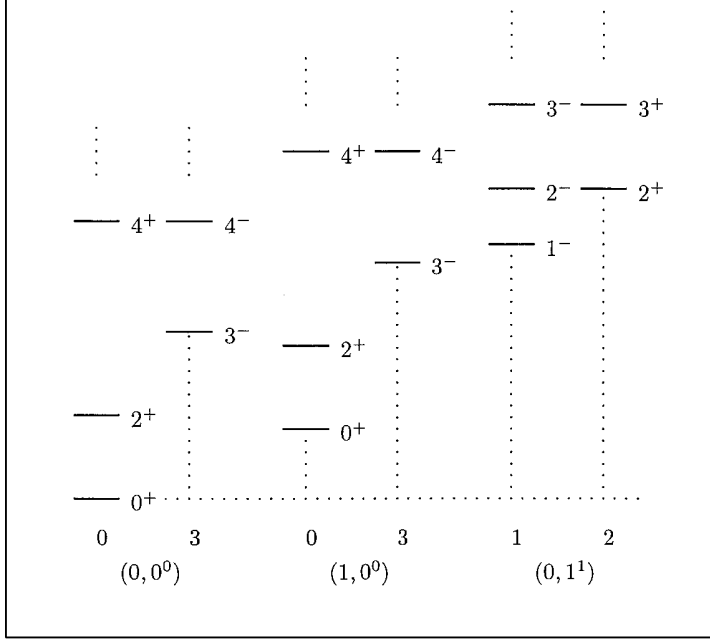


**FIG. 4.** Schematic spectrum of an oblate symmetric top. All states are symmetric under $S_3$.

In Fig. 4 we show the structure of the spectrum of the oblate top according to the approximate energy formula of Eq. (5.19). The energy spectrum consists of a series of rotational bands labeled by $(v_1, v_2^{\ell_2})$ and $K$. The degeneracy between states with different values of $K$ can be split by the last term in Eq. (5.19).

## 6. TRANSITION PROBABILITIES

In order to calculate transition form factors in the algebraic cluster model one has to express the transition operator in terms of the algebraic operators. In the large $N$ limit, the $U(7)$ dipole operators $\hat{D}_\rho$ and $\hat{D}_\lambda$ of Eq. (4.10) correspond to the Jacobi coordinates [21]. The matrix elements of $\exp(-iq\sqrt{2/3}\lambda_z)$ can be obtained algebraically by making the replacement [15]

$$\sqrt{2/3}\lambda_z \to \beta \hat{D}_{\lambda,z}/X_D, \tag{6.1}$$

where $\beta$ represents the scale of the coordinate and $X_D$ is given by the reduced matrix element of the dipole operator [15]. In summary, the transition form factors can be expressed in the ACM as

$$\mathcal{F}(i \to f; q) = \langle \gamma_f, L_f, M | \hat{T} | \gamma_i, L_i, M \rangle, \tag{6.2}$$

with

$$\hat{T} = e^{i\epsilon \hat{D}_{\lambda,z}} = e^{-iq\beta \hat{D}_{\lambda,z}/X_D}. \tag{6.3}$$

in which the form factors are obtained exactly by using the symmetry properties of the transition operator of Eq. (6.3) (see Appendix D of [15]).

### 6.1. Dynamic Symmetries

When a dynamic symmetry occurs the matrix elements of the transition operators can be obtained in explicit analytic form. The general procedure to derive the transition form factors in the $U(6)$ and $SO(7)$ limits has been discussed in [15, 23].

In the $U(6)$ limit, the elastic form factor is given by [15]

$$\mathcal{F}(0_1^+ \to 0_1^+; q) = (\cos\epsilon)^N \to e^{-q^2\beta^2/6}. \tag{6.4}$$

In the last step we have taken the large $N$ limit such that $\epsilon X_D = \epsilon\sqrt{3N} = -q\beta$ remains finite. For the extended charge distribution, the form factor of Eq. (6.4) is multiplied by a Gaussian $\exp(-q^2/4\alpha)$. The coefficients $\beta$ and $\alpha$ cannot be determined independently, since both have the same dependence on $q^2$. The charge radius can be used to fix one particular combination

$$\langle r^2\rangle^{1/2} = \sqrt{\frac{3}{2\alpha} + \beta^2}. \tag{6.5}$$

In Table II we show the results for some transition form factors in the $U(6)$ limit of the ACM. In the large $N$ limit, they reduce to those obtained for the harmonic oscillator of Table I. All form factors exhibit an exponential fall-off with momentum transfer. In Fig. 5 we show the elastic form factor in the large $N$ limit (solid line). The coefficients $\beta$ and $\alpha$ were taken to give the charge radius of $^{12}$C: $\langle r^2\rangle^{1/2} = 2.468$ fm [24]. The corresponding charge distribution shows an exponential decay with $r$ (solid line in Fig. 6).

TABLE II

Transition Form Factors $\mathcal{F}(0_1^+ \to L_i^P; q)$ for the $U(6)$ Limit of the Algebraic Cluster Model

| $L_i^P$ | $\mathcal{F}(0_1^+ \to L_i^P; q)$ |
|---|---|
| $0_1^+$ | $(\cos\epsilon)^N$ |
| $0_2^+$ | $\sqrt{\frac{N!}{12(N-2)!}}\,(\cos\epsilon)^{N-2}(i\sin\epsilon)^2$ |
| $1_1^-$ | $\sqrt{\frac{N!}{40(N-3)!}}\,(\cos\epsilon)^{N-3}(i\sin\epsilon)^3$ |
| $2_1^+$ | $\sqrt{\frac{N!}{6(N-2)!}}\,(\cos\epsilon)^{N-2}(i\sin\epsilon)^2$ |
| $3_1^-$ | $\sqrt{\frac{N!}{60(N-3)!}}\,(\cos\epsilon)^{N-3}(i\sin\epsilon)^3$ |
| $4_1^+$ | $\sqrt{\frac{N!}{280(N-4)!}}\,(\cos\epsilon)^{N-4}(i\sin\epsilon)^4$ |

*Note*. The coefficient $\epsilon$ is given by $\epsilon = -q\beta/\sqrt{3N}$.

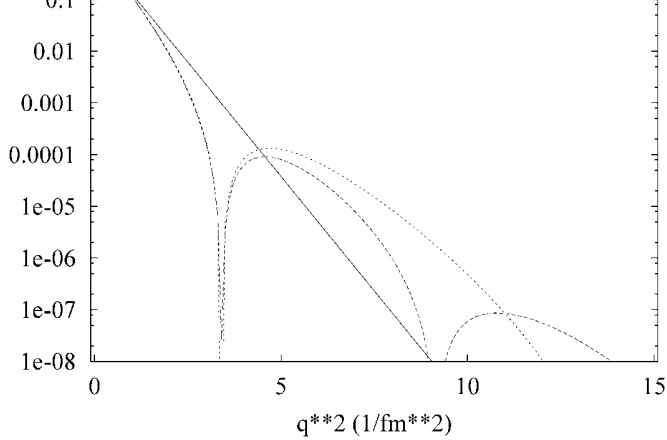


**FIG. 5.** Comparison of the elastic form factor $|\mathcal{F}(0_1^+ \to 0_1^+; q)|^2$, calculated for $N \to \infty$ (a) in $U(6)$ with $\beta = 1.70$ fm and $\alpha = 0.47$ fm$^{-2}$ (solid line), (b) in $SO(7)$ with $\beta = 1.97$ fm and $\alpha = 0.67$ fm$^{-2}$ (dashed line), (c) in the oblate top with $\beta = 1.70$ fm and $\alpha = 0.47$ fm$^{-2}$ (dotted line).

For the $SO(7)$ symmetry, the transition form factors can be expressed in terms of Gegenbauer polynomials or, equivalently, hypergeometric funcions. For the elastic form factor we have [17]

$$\mathcal{F}(0_1^+ \to 0_1^+; q) = \frac{4!N!}{(N+4)!} C_N^{(5/2)}(\cos\epsilon)$$
$$= {}_2F_1\left(-\frac{N}{2}, \frac{N+5}{2}, 3; \sin^2\epsilon\right) \to \frac{4J_2(q\beta\sqrt{2})}{q^2\beta^2}. \tag{6.6}$$

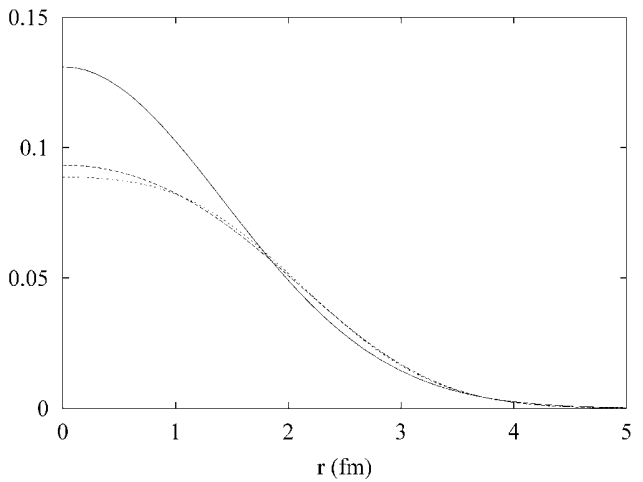


**FIG. 6.** Ground state charge distribution $\rho(r)$ (fm$^{-3}$) calculated for $N \to \infty$ (a) in $U(6)$ with $\beta = 1.70$ fm and $\alpha = 0.47$ fm$^{-2}$ (solid line), (b) in $SO(7)$ with $\beta = 1.97$ fm and $\alpha = 0.67$ fm$^{-2}$ (dashed line), (c) in the oblate top with $\beta = 1.70$ fm and $\alpha = 0.47$ fm$^{-2}$ (dotted line).

of the Algebraic Cluster Model

| $L_i^P$ | $\mathcal{F}(0_1^+ \to L_i^P; q)$ |
|---|---|
| $0_1^+$ | $\frac{4!N!}{(N+4)!} C_N^{(5/2)}(\cos\epsilon)$ |
| $0_2^+$ | 0 |
| $1_1^-$ | $\sqrt{\frac{189N!(N-3)!10!}{(N+4)!(N+7)!}} (i\sin\epsilon)^3 C_{N-3}^{(11/2)}(\cos\epsilon)$ |
| $2_1^+$ | $\sqrt{\frac{140N!(N-2)!8!}{(N+4)!(N+6)!}} (i\sin\epsilon)^2 C_{N-2}^{(9/2)}(\cos\epsilon)$ |
| $3_1^-$ | $\sqrt{\frac{126N!(N-3)!10!}{(N+4)!(N+7)!}} (i\sin\epsilon)^3 C_{N-3}^{(11/2)}(\cos\epsilon)$ |
| $4_1^+$ | $\sqrt{\frac{297N!(N-4)!12!}{(N+4)!(N+8)!}} (i\sin\epsilon)^4 C_{N-4}^{(13/2)}(\cos\epsilon)$ |

*Note*. The coefficient $\epsilon$ is given by $\epsilon = -q\beta/\sqrt{N(N+5)/2}$.

The normalization constant is given by $X_D = \sqrt{N(N+5)/2}$. Again, in the last step we have taken the large $N$ limit such that $\epsilon X_D = -q\beta$ remains finite. The $SO(7)$ transition form factors are presented in Table III. In the large $N$ limit, they reduce to those obtained for the deformed oscillator of Table I. All form factors exhibit an oscillatory behavior. The transition form factor to the first excited $0^+$ state which belongs to a vibrational excitation $v = (N-\omega)/2 = 1$ vanishes identically, since the dipole operator is a generator of $SO(7)$. In Fig. 5 we show the elastic form factor for $N \to \infty$ (dashed line). The values of $\beta$ and $\alpha$ are taken to reproduce the minimum in the elastic form factor of $^{12}$C at $q^2 = 3.4$ fm$^{-2}$ and the $^{12}$C charge radius of 2.468 fm. The corresponding charge distribution for the deformed oscillator is given by the dashed line in Fig. 6.

### 6.2. Oblate Symmetric Top

For the oblate symmetric top, the form factors can only be obtained in closed form in the large $N$ limit [15] (see Table I). As an example, the elastic form factor has been obtained as [15, 18]

$$\mathcal{F}(0_1^+ \to 0_1^+; q) \to j_0(q\beta). \tag{6.7}$$

In this case, the normalization constant is given by $X_D = NR\sqrt{2}/(1+R^2)$. As can be seen from the last column of Table I, all form factors show an oscillatory behavior. In Fig. 5 we show the elastic form factor in the large $N$ limit (dotted line). The coefficients $\beta$ and $\alpha$ have been determined to give the same value of the minimum and the charge radius as for the deformed oscillator. The charge distribution for the oblate top is given by Eq. (3.26) and is represented by the dotted line in Fig. 6.

The transition form factors for vibrational excitations are proportional to the corresponding intrinsic transition matrix elements $\chi_1$ and $\chi_2$ for each type of vibration $v_1$ and $v_2$, respectively [8]

$$\begin{aligned} \chi_1 &= \frac{1-R^2}{2R\sqrt{N}}, \\ \chi_2 &= \frac{\sqrt{1+R^2}}{R\sqrt{2N}}. \end{aligned} \tag{6.8}$$

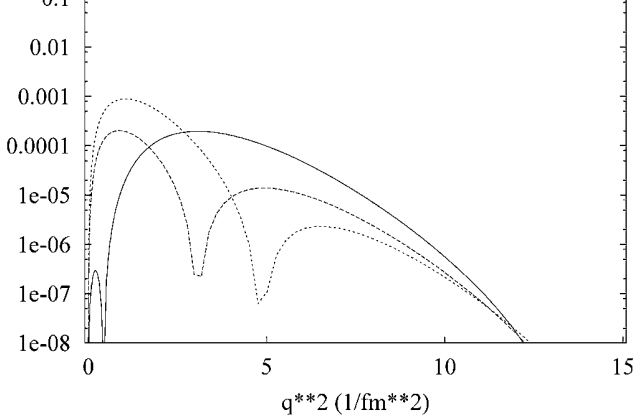


**FIG. 7.** Inelastic form factor $|\mathcal{F}(0_1^+ \to 0_2^+; q)|^2$ for the oblate top, calculated for $N = 10$ and $R^2 = 0.5$ (solid line), 1.0 (dashed line), and 1.5 (dotted line).

In Fig. 7 we show the inelastic form factor $|\mathcal{F}(0_1^+ \to 0_2^+; q)|^2$ for different values of $R^2$. As before, the coefficients $\beta$ and $\alpha$ are determined by the first minimum of the elastic form factor and the charge radius. Whereas the elastic form factor does not depend on $R^2$, the inelastic form factor is very sensitive to the value of $R^2$, especially with respect to the position of its minimum.

## 7. THE NUCLEUS $^{12}$C

The structure of $^{12}$C has been extensively investigated since the early days of nuclear physics. Comprehensive calculations of $^{12}$C have been done within the framework of the shell model, starting with the early calculation of Cohen and Kurath [25] in the $p$-shell and ending with the more recent calculations with large shell mixing. $^{12}$C has also been the battleground for investigations within the framework of the microscopic cluster model. Here we investigate the extent to which properties of the low-lying spectrum of $^{12}$C can be described in terms of the macroscopic cluster model. The reason why a detailed analysis is now feasible is two-fold. First, we have a set of explicit analytic formulas for energies, electromagnetic transition rates and form factors for the oblate top that can be easily compared with experiments. Second and foremost is that the development of the algebraic cluster model allows us to study in a straighforward way complex situations, such as those that are not rigid, but correspond for example to situations which are intermediates between two limiting cases.

The differences between the three special solutions of the ACM, the $U(6)$ limit, the $SO(7)$ limit, and the oblate top, are most pronounced in the transition form factors. The elastic form factor of $^{12}$C shows a minimum at $q^2 = 3.4$ fm$^{-2}$ and no further structure up to about $q^2 \sim 14$ fm$^{-2}$. Also the inelastic form factor for the transition $0_1^+ \to 0_2^+$ shows a clear minimum at $\sim q^2 = 4.5$ fm$^{-2}$. The analysis of the form factors that was presented in the previous section shows clearly that only the oblate top scenario can account for the features of the empirical form factors of $^{12}$C. In the $U(6)$ limit the form factors drop off exponentially and have no minima, whereas in the $SO(7)$ limit the inelastic form factor vanishes identically.

Therefore, in this section we analyze the spectroscopy of $^{12}$C in the oblate top limit of the ACM.

the Energy Spectrum and the Transition Form Factors of $^{12}C$

| | | |
|---|---|---|
| $\xi_1$ | 0.1721 | MeV |
| $\xi_2$ | 0.2745 | MeV |
| $\kappa_1$ | 0.7068 | MeV |
| $\kappa_2$ | 0.1276 | MeV |
| $R^2$ | 1.40 | |
| $\beta$ | 1.74 | fm |
| $\alpha$ | 0.52 | $fm^{-2}$ |

*Note*. The number of bosons is $N = 10$.

### 7.1. Energies

The Hamiltonian for the oblate top is given by Eq. (4.13). The coefficients $\xi_1$, $\xi_2$, $\kappa_1$, and $\kappa_2$ are determined in a fit to the excitation energies of $^{12}C$ (see Table IV). The number of bosons is taken to be $N = 10$. In Fig. 8 we show a comparison between the experimental data and the calculated states of the oblate top with energies $<15$ MeV. One can clearly identify in the experimental spectrum the states $0^+$, $2^+$, $3^-$, $4^+$ of the ground rotational band, the state $0^+$ of the stretching vibration, and the state $1^-$ of the bending vibration. However, the $3^-$ state does not fall at the location expected from a rigid extended configuration with moments of inertia given by Eq. (2.7), but at a higher excitation energy. Since the $3^-$ state has $K = 3$ the deviation from the simple rotational formula indicates large rotation–vibration interactions. This conclusion is strengthened by the low location of the stretching vibration. In contrast with molecules, the vibrational and rotational frequencies in nuclei appear to be comparable. If one takes as a measure of the ratio $E_{\text{vib}}/E_{\text{rot}}$ the quantity $E_{0_2^+}/E_{2_1^+}$, this quantity is 1.7 in $^{12}C$ and $\sim 10$ in a typical molecule with $\mathcal{D}_{3h}$ symmetry (for example, ozone $O_3$).

### 7.2. Form Factors and Transition Rates

Form factors for electron scattering on $^{12}C$ were measured long ago. For the extended charge distribution of Eq. (2.23), the form factors are obtained by multiplying the oblate top form factors by an exponential factor $\exp(-q^2/4\alpha)$ (compare Eqs. ((2.20) and (2.24)). The coefficient $\beta$ is determined from the first minimum in the elastic form factor at $q^2 = 3.4$ $fm^{-2}$ [24] to be $\beta = 1.74$ fm, and subsequently the coefficient $\alpha$ is determined from the charge radius of $^{12}C$, $\langle r^2 \rangle^{1/2} = 2.468 \pm 0.012$ fm [24], to be $\alpha = 0.52$ $fm^{-2}$. If the alpha particles would not be effected by the presence

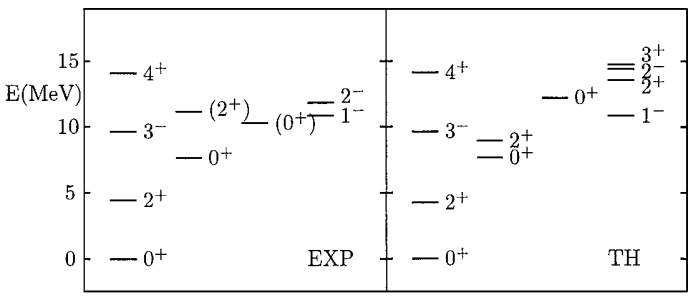


**FIG. 8.** Comparison between the low-lying experimental spectrum of $^{12}C$ [26] and that calculated with the oblate top Hamiltonian of Eq. (4.13) with $N = 10$. The parameter values are given in Table IV. States with uncertain spin-parity assignment are in parentheses.

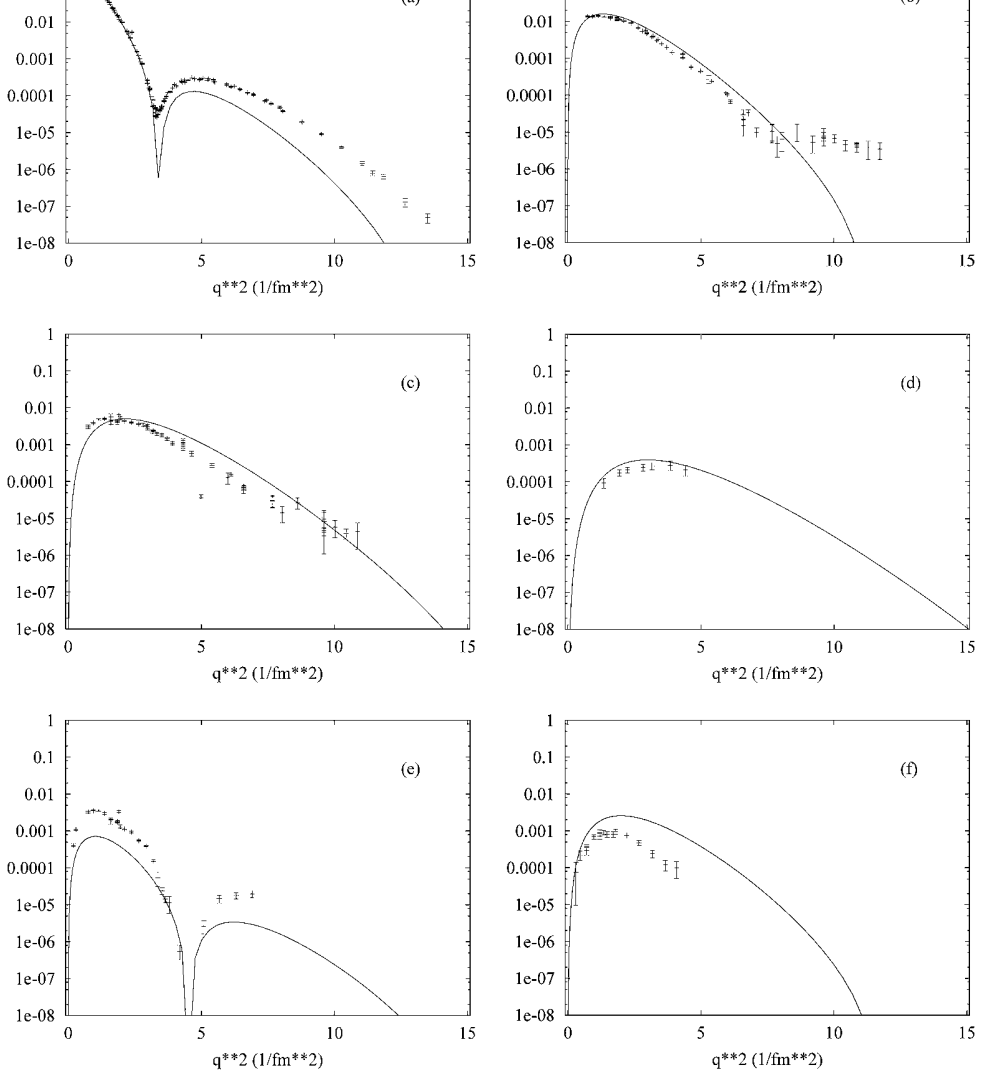


**FIG. 9.** Comparison between the experimental form factors $|\mathcal{F}(0_1^+ \to L_i^P; q)|^2$ of $^{12}$C for the final states (a) $L_i^P = 0_1^+$ (elastic), (b) $L_i^P = 2_1^+$, (c) $L_i^P = 3_1^-$, (d) $L_i^P = 4_1^+$, (e) $L_i^P = 0_2^+$, and (f) $L_i^P = 1_1^-$ and those obtained for the oblate top with $N = 10$. The parameter values are given in Table IV. The experimental data are taken from [24] and [27]–[32].

of the others, the coefficient $\alpha$ should be the same as for free particles. The value of $\alpha$ is slightly different from the one used in [9], where it was determined from the maximum in the elastic form factor.

In Fig. 9 we show a comparison between experimental and theoretical form factors calculated exactly using the Hamiltonian of Eq. (4.13). The value of the parameters of the Hamiltonian and the transition operator is given in Table IV. We note that the transition form factors are calculated with the same values of coefficients $\alpha$ and $\beta$ as determined from the elastic form factor. Whereas for the rotational excitations the calculations seem to give a good description of the experimental data, the

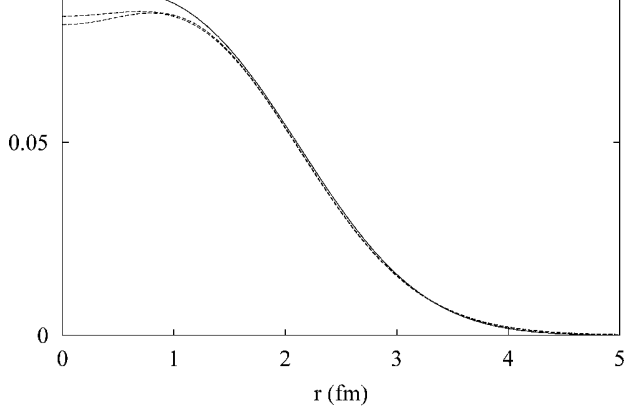


**FIG. 10.** Comparison between the ground state charge distribution $\rho(r)$ (fm$^{-3}$) of $^{12}$C extracted from the experimental elastic form factor (dashed lines) [24] and that calculated for the oblate top with $N = 10$ (solid line). The parameter values are given in Table IV.

situation is different for vibrational excitations. Although the $q$ dependence of the vibrational form factors is consistent with the experiment, indicating that the $0_2^+$ and $1_1^-$ excited states could indeed be the vibrational excitations of a three-alpha configuration with $\mathcal{D}_{3h}$ symmetry, their observed large strength implies a very large mixing with other configurations. The strengths of these excitations are proportional to the corresponding intrinsic transition matrix elements $\chi_1$ and $\chi_2$ for each type of vibration $v_1$ and $v_2$, respectively [8]. According to Eq. (6.8), the coefficients $\chi_1$ and $\chi_2$ go to zero in the large $N$ limit (rigid configurations). For finite values of $N$, the vibrational transition form factors are different from zero. The solid lines in Figs. 9 were obtained in calculations for a finite value of $N = 10$.

From the form factors one can extract other electromagnetic properties of interest. The ground state charge distribution can be obtained by taking the Fourier transform of the elastic form factor according to Eq. (3.25). In Fig. 10 we compare the charge distribution of $^{12}$C obtained from the calculated elastic form factor of Fig. 9 and extracted in a Fourier–Bessel analysis of the experimental data [24].

The $B(EL)$ values correspond to the long wavelength limit of the form factors (see Eq. (3.23)). The values extracted from the fit to the form factors are shown in Table V. For the monopole strength, instead of $B(E0)$ it is customary to give the matrix element $M(E0)$. While the $B(E2; 2_1^+ \to 0_1^+)$ and

TABLE V

Comparison between Calculated (Th.) and Measured (Exp.) Values

| | Th. | Exp. | | Ref. |
|---|---|---|---|---|
| $B(E2; 2_1^+ \to 0_1^+)$ | 8.4 | $7.6 \pm 0.4$ | $e^2\text{fm}^4$ | [26] |
| $B(E3; 3_1^- \to 0_1^+)$ | 44 | $103 \pm 17$ | $e^2\text{fm}^6$ | [26] |
| $B(E4; 4_1^+ \to 0_1^+)$ | 73 | | $e^2\text{fm}^8$ | |
| $B(E2; 0_2^+ \to 2_1^+)$ | 1.3 | $13.1 \pm 1.8$ | $e^2\text{fm}^4$ | [26] |
| $M(E0; 0_2^+ \to 0_1^+)$ | 0.4 | $5.5 \pm 0.2$ | fm$^2$ | [30] |
| $\langle r^2 \rangle^{1/2}$ | 2.468 | $2.468 \pm 0.12$ | fm | [24] |

a vibrational mode.

## 8. CONCLUSIONS

In this article, we have presented a detailed analysis of a configuration composed of three alpha particles at the vertices of an equilateral triangle. We have done so in a classical, quantum, and quantum algebraic description. The formulas that have been derived have been used to study the ground state configuration of $^{12}$C. In addition, we have introduced a new method to study clustering based on the algebraic quantization of the Jacobi variables. The latter method is very general and it allows us to describe in a relatively simple fashion not only three particles at the vertices of a triangle (oblate top) but also other situations such as six-dimensional vibrations and rotational–vibrational spectra.

Our analysis of the experimental data for $^{12}$C appears to indicate that the triangular configuration describes the data (energy levels and form factors) reasonably well for the rotational band $0_1^+, 2_1^+, 3_1^-, 4_1^+$, although with large rotation–vibration interactions. The situation is different for the vibrational excitations $0_2^+$ and $1_1^-$. Here the shape of the form factors is well reproduced but its magnitude is not.

We call attention to the quantum algebraic description in terms of the algebra of $U(7)$ that is capable of describing not only rigid like structures but also floppy structures. We point out that this method is very general and can describe other situations such as, for example, three alpha particles on a line. These configurations cannot describe the low-lying experimental spectrum of $^{12}$C since for three alpha particles on a line there are (in the ground rotational band) no negative parity states. They may occur as excited configurations. Their properties will be presented in a forthcoming publication. The crucial problem in clustering in nuclei is to understand what type of configurations are present, if any, and to provide unambiguous experimental evidence for these configurations. The algebraic method gives a way in which all calculations can be performed easily.

Finally, the general algebraic framework based on the spectrum generating algebra $U(7)$ also allows us to describe clustering phenomena for three different particles [33]. This description is relevant to giant trinuclear molecules in ternary cold fission [34, 35].

## ACKNOWLEDGMENTS

It is a pleasure to thank Aurora Tumino for her help in calculating the form factors of $^{12}$C. This work was supported in part by CONACyT under Project 32416-E by DPAGA under Project IN106400, and by D.O.E. Grant DE-FG02-91ER40608.

## REFERENCES

1. J. A. Wheeler, *Phys. Rev.* **52** (1937), 1083.
2. K. Wildermuth and Th. Kanellopoulos, *Nucl. Phys.* **7** (1958), 150.
3. K. Ikeda, H. Horiuchi, and S. Sato, *Suppl. Progr. Theor. Phys.* **68** (1980), 1.
4. Y. Fujiwara, H. Horiuchi, K. Ikeda, M. Kamimura, K. Kato, Y. Suzuki, and E. Uegaki, *Suppl. Progr. Theor. Phys.* **68** (1980), 29.
5. H. Horiuchi, *Prog. Theor. Phys.* **51** (1974), 1266; *Prog. Theor. Phys.* **53** (1975), 447.
6. F. Iachello, *in* "Lie Algebras, Cohomologies and New Applications of Quantum Mechanics" (N. Kamran and P. Olver, Eds.), Contemporary Mathematics, Vol. 160, p. 151, Amer. Math. Soc., Providence, RI, 1994.
7. F. Iachello, *Phys. Rev. C* **23** (1981), 2778.
8. R. Bijker and F. Iachello, *Phys. Rev. C* **61** (2000), 067305.

2000.
10. G. Herzberg, “Molecular Spectra and Molecular Structure II: Infrared and Raman Spectra of Polyatomic Molecules,” Van Nostrand, New York, 1950.
11. J. D. Jackson, “Classical Electrodynamics,” Wiley, New York, 1962.
12. F. T. Smith, *Phys. Rev.* **120** (1960), 1058.
13. J. L. Ballot and M. Fabre de la Ripelle, *Ann. Phys. (N.Y.)* **127** (1980), 62.
14. G. De Franceschi, F. Palumbo, and N. Lo Iudice, *Phys. Rev. C* **29** (1984), 1496.
15. R. Bijker, F. Iachello, and A. Leviatan, *Ann. Phys. (N.Y.)* **236** (1994), 69.
16. L. A. Copley, G. Karl, and E. Obryk, *Nucl. Phys. B* **13** (1969), 303; F. E. Close and Z. Li, *Phys. Rev. D* **42** (1990), 2194.
17. R. Bijker and A. Leviatan, *Rev. Mex. Fís.* **44 S2** (1998), 15.
18. E. V. Inopin and B. I. Tishchenko, *Soviet Physics, JEPT* **11** (1960), 840.
19. R. Bijker, Computer program ACM, unpublished.
20. J. N. Ginocchio and M. Kirson, *Phys. Rev. Lett.* **44** (1980), 1744; A. E. L. Dieperink, O. Scholten, and F. Iachello, *Phys. Rev. Lett.* **44** (1980), 1747.
21. O. S. van Roosmalen and A. E. L. Dieperink, *Ann. Phys. (N.Y.)* **139** (1982), 198.
22. R. Bijker, A. E. L. Dieperink, and A. Leviatan, *Phys. Rev. A* **52** (1995), 2786.
23. R. Bijker and J. N. Ginocchio, *Phys. Rev. C* **45** (1992), 3030.
24. W. Reuter, G. Fricke, K. Merle, and H. Miska, *Phys. Rev. C* **26** (1982), 806.
25. S. Cohen and D. Kurath, *Nucl. Phys.* **73** (1965), 1.
26. F. Ajzenberg-Selove, *Nucl. Phys. A* **506** (1990), 1.
27. I. Sick and J. S. McCarthy, *Nucl. Phys. A* **150** (1970), 631.
28. H. L. Crannell and T. A. Griffy, *Phys. Rev.* **136** (1964), B1580.
29. H. Crannell, *Phys. Rev.* **148** (1966), 1107.
30. P. Strehl and Th. H. Schucan, *Phys. Lett. B* **27** (1968), 641.
31. Y. Torizuka, M. Oyamada, K. Nakahara, K. Sugiyama, Y. Kojima, T. Terasawa, K. Itoh, A. Yamaguchi, and M. Kimura, *Phys. Rev. Lett.* **22** (1969), 544.
32. A. Nakada, Y. Torizuka, and Y. Horikawa, *Phys. Rev. Lett.* **27** (1971), 745 and 1102.
33. R. Bijker and A. Leviatan, *Few-Body Systems* **25** (1998), 89.
34. Ş. Mişicu, P. O. Hess, and W. Greiner, *Phys. Rev. C* **63** (2001), 054308.
35. R. Bijker, P. O. Hess, and Ş. Mişicu, *Heavy Ion Physics* **13** (2001), 89; P. O. Hess, R. Bijker, and Ş. Mişicu, *Rev. Mex. Fís.* **47 S2** (2001), 52.